Nanoscale

Accepted Manuscript

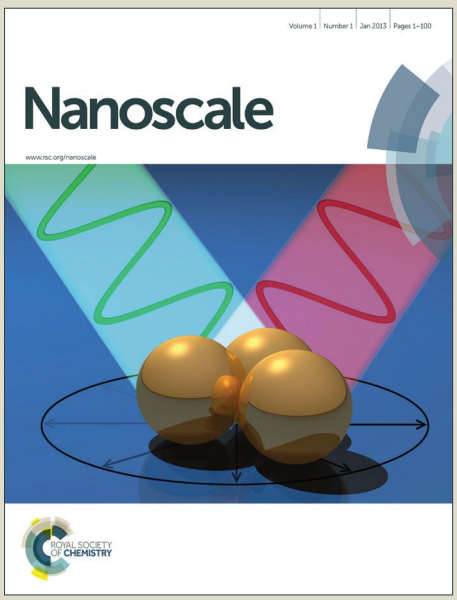

ROYAL SOCIETY OF CHEMISTRY

www.rsc.org/nanoscale

Planar Plasmonic Chiral Nanostructures

*Shuai Zu[1], Yanjun Bao[1], and Zheyu Fang[1,2]**

[1]School of Physics, State Key Lab for Mesoscopic Physics, Peking University, Beijing 100871, China.

[2]Collaborative Innovation Center of Quantum Matter, Beijing 100871, China.

Email: zhyfang@pku.edu.cn

A strong chiral optical response induced at a plasmonic Fano resonance in a planar Au heptamer nanostructure was experimentally and theoretically demonstrated. The scattering spectra show the characteristic narrow-band feature of Fano resonances for both left and right circular polarized lights, with a chiral response reaching 30% at the Fano resonance. Specifically, we systematically investigate the chiral response of planar heptamers with gradually changing the inter-particle rotation angles and separation distance. The chiral spectral characteristics clearly depend on the strength of Fano resonance and associated near-field optical distributions. Finite element method simulations together with a multipole expansion method demonstrate that the enhanced chirality is caused by the excitation of magnetic quadrupolar and electric toroidal dipolar modes. Our work provides an effective method for the design of 2D nanostructures with strong chiral response.

KEYWORDS: Chirality, Surface Plasmons, Multiple Modes, Circular Polarization Light, Nanostructure.

Metallic nanostructures as simple and versatile platforms for control and manipulation of electromagnetic fields at the nanoscale is currently an active research area. Their optical resonances are determined by collective electron oscillations known as surface plasmon resonance (SPR)[1, 2, 3]. The SPR resonances depend sensitively on the geometry, material and dielectric environment[4, 5], making it possible to design nanoscale structures with high sensitivity to the chiral state of light[6, 7, 8, 9] and possible uses in biosensing applications such as protein sensing[10, 11]. Three-dimensional (3D) metallic chiral structures, inherently have a large light-matter interaction volume allowing sufficiently strong interaction between electric and magnetic modes to result in large circular dichroism (CD)[12, 13, 14, 15]. However, the fabrication of nanostructured 3D chiral materials is challenging using conventional top-down approaches which inherently are based on 2D patterning. DNA-based chiral assemblies from solution phase system maybe another solution for the fabricating complex 3D structures, but it is difficult to create large-area regular arrays[16, 17]. For this reason significant effort has been devoted to the development of two-dimensional (2D) chiral metamaterials, such as gammadions[18, 19], G-shape[20] and S-shape structures[21]. However, such nanostructures with their obvious geometric chirality usually exhibit only small CD[22].

Great efforts have been made to enhance and explain the optical chirality in periodic structure through symmetry analysis and design[23, 24]. However, this task

remains challenging for individual 2D plasmonic nanostructures with their reduced light-matter interaction volume. In several recent applications it has been shown that plasmonic Fano interference can strongly enhance the strength of light-matter interactions in individual metallic nanostructures[25, 26]. This enhancement is due to the indirect coupling between bright and dark collective modes that can provide large local electromagnetic field enhancements and strong near-field couplings. Successful applications of this approach include the development of substrates for enhanced LSPR sensing[27, 28, 29], Raman Scattering[30, 31], photodetection[32, 33], and nonlinear optics effects[34, 35].

In this work, we show that plasmonic Fano interference can dramatically enhance the light-matter interaction in individual metallic nanostructures and resulting in a strong narrow-band chiral optical response. The inter-particle rotation angle and separation distance of the planar heptamers are controlled in order to achieve a maximum optical chirality. To explain the experimental results, we use finite element method (FEM) simulations combined with a multipole expansion method, which provides insight into the underlying chirality mechanism and pave the way for the further optimization and tuning of the chiral response of 2D interacting plasmonic nanostructures.

Results

Design of planar plasmonic chiral heptamer. The schematic of the planar heptamer structure is shown in Fig. 1a., consisting of a central disk with radius r = 85 nm and

six satellite ellipses with major axis a = 85 nm and minor axis b = 35 nm. This chiral nanostructure was fabricated on a SiO_2/Si substrate using E-beam lithography following Au evaporation (30 nm thickness) and is shown in the SEM picture as Fig. 1b. The orientations and positions of the surrounding ellipses have their centers located at the vertexes and the major axes parallel to the side directions of a regular hexagon with side length d = 180 nm. The structure was normal-illuminated with focused left-handed (LCP) or right-handed (RCP) circularly polarized light that generated by a quarter-wave plate and a linear polarizer. The scattering spectra were measured using dark-field optical microscopy (See Text S1 in the Supplementary Information) and is shown in Fig. 1c.

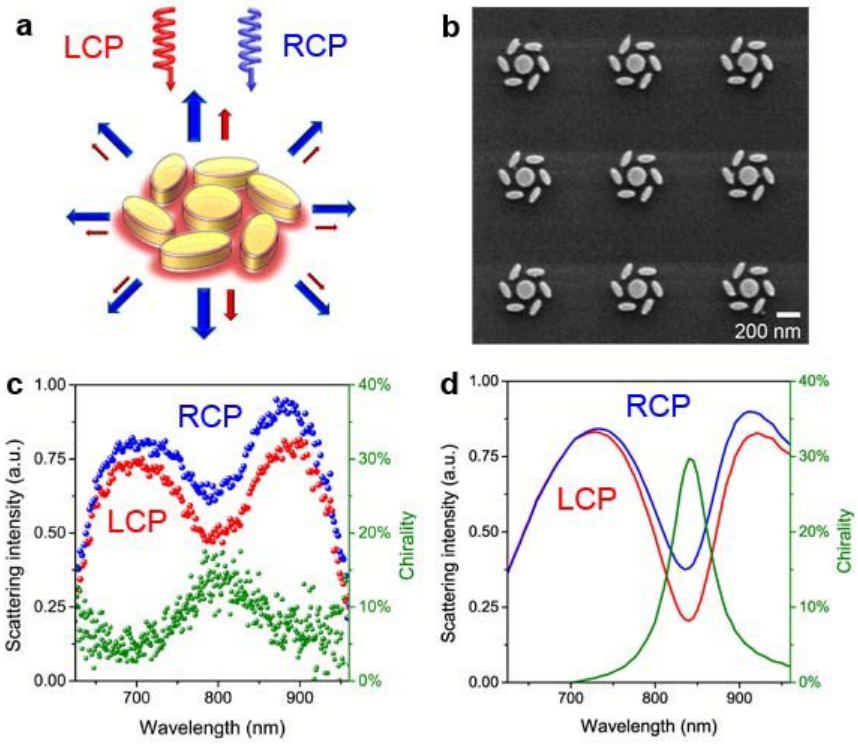

Figure 1. (a) Schematic of the chiral Fano oligomer under normal-incident circularly polarized light. (b) SEM image for the heptamer consisting of a central disk (r = 85 nm) and six satellite ellipses with major axis 85 nm and minor axis 35 nm. (c) Measured dark-field scattering spectra for LCP (red) and RCP (blue) excitation, and its corresponding optical chirality (green). (d)

Scattering cross section calculated for LCP and RCP incidence and the resulting chirality.

A pronounced plasmonic Fano resonance appears at 800 nm for both LCP and RCP excitations. And a prominent scattering intensity difference at the Fano dip is apparent, indicating a strong optical chirality. To quantify the CD, we define an optical chirality (OC) as $\left|(\sigma_{sca}^{\mathrm{LCP}}-\sigma_{sca}^{\mathrm{RCP}})/(\sigma_{sca}^{\mathrm{LCP}}+\sigma_{sca}^{\mathrm{RCP}})\right|\times 100\%$, where $\sigma_{sca}^{\mathrm{LCP(RCP)}}$ is the scattering cross section under LCP (RCP) excitation. Using this definition, the optical chirality is found to be strongly wavelength dependent and with its maximum as about 20% at the Fano resonance, which is much higher than what is typically observed for common planar nanostructures[22, 36]. Numerical simulations were also performed using the finite element method (FEM) to simulate the scattering cross section of the fabricated structure. The simulation domain includes the structure with perfect matched layers in all directions. The Au dielectric function was obtained from Johnson and Christy[37], and the refractive index of SiO_2 is n=1.45. The entire structure is illuminated by a normal-incident circularly polarized light with the electric field in the *xy*-plane. Fig. 1d shows the calculated scattering cross section of the chiral Fano oligomers under LCP (red line) and RCP (blue line) illumination, which has good agreement with the experimental measurements, where the Fano resonance emerge in the scattering spectra for both polarizations, but is much deeper for LCP illumination. The absorption cross section was also calculated and found to be larger for LCP than for RCP at the Fano resonance (See Fig. S1 in the Supplementary Information). These characteristics in both the scattering and absorption spectra indicate that Fano interference is strongest for LCP excitation. The sample without substrate was also

simulated, with the similar scattering spectra, the influence induced by the substrate can be ruled out. (See Fig. S2 in the Supplementary Information)

Chiral response with ellipse rotation angle. In order to investigate the influence of the structure symmetry on the optical chirality, we fabricated a series of planar heptamers with various inter-particle rotation angle as shown in Fig. 2. The inter-particle rotation angles is defined as θ (See Fig. 3a), and changed from 30 to 180 degree. The corresponding SEM images for each of the structure are displayed on the top of curve plots. The measured scattering spectra are displayed and compared in Fig. 2 for both LCP (light gray) and RCP (gray) excitation.

Under each of the rotation angle, the corresponding optical chirality was measured. The plasmonic Fano resonance was found first blue shift and then red shift with the increasing of the rotation angle θ under either LCP or RCP illumination. With the largest structure symmetry breaking, the maximum chirality was recorded when θ is 60° and 180°. The chirality decreases with the decreasing of the symmetry breaking, and finally disappear when the θ changed to 30° and 120°. Because of the weak coupling between the center disk dipolar mode and the satellite ellipses long-axis dipolar mode, the strength of the Fano resonance dramatically reduced when θ is 120°. These results show that the planar heptamers have a well-functioned spectral tunability and robust optical chirality. FEM simulations were performed and calculated the scattering cross section of these fabricated structures. All of the main spectral features are clearly confirmed, and the deviation between the experiment and

simulations possibly is induced by the sample nanofabrication. (See Fig. S3 in the Supplementary Information)

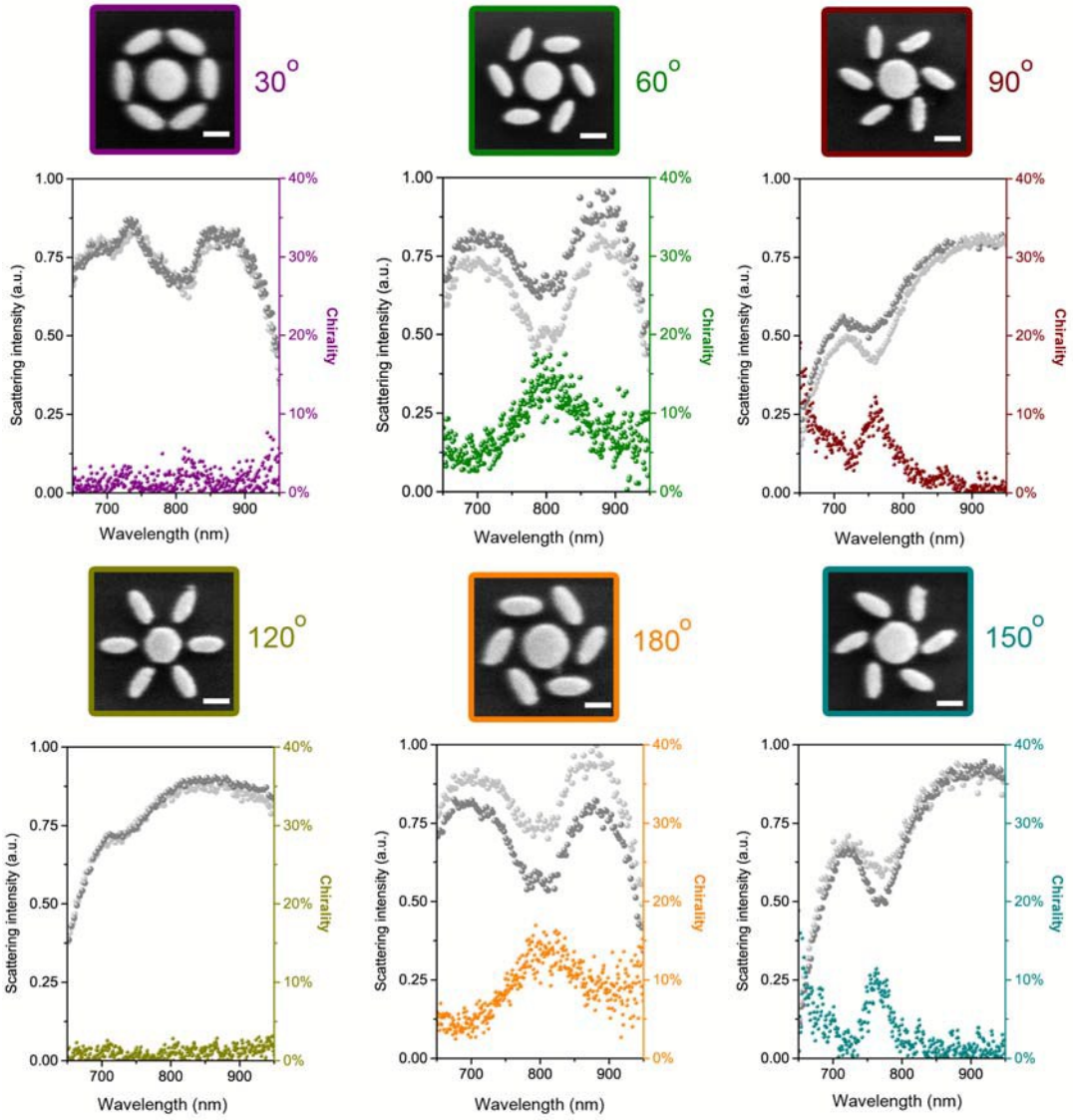

Figure 2. The rotation angle θ is changed from 30 to 180 degree, and for each of the oligomer structure, the corresponding SEM images are on the top of the scattering spectra. With the largest structure symmetry breaking, the Chirality reaches ~20% when θ is 60 and 180 degree. The Chirality decreases to ~10% with the increasing of the structure symmetry, as θ = 90 and 150 degree, and finally disappear when θ changes to 30 and 120 degree. The scale bar is 200 nm.

Chiral response with inter-particle distance. The heptamer nanostructures with various inter-particle distances were further fabricated and investigated for the plasmon coupling on the optical chirality. The gap distance *d* is changed from 160 to 260 nm, as shown in the SEM images of Fig. 3a. From Fig. 3b, we can see that with a large inter-particle distance, such as *d* = 260 nm or even larger, the measured scattering spectra show the similar dipolar resonance around 800 nm because of the weak coupling between the center disk and the surrounding nano-ellipses. As *d* decreases to the 220 nm, plasmonic Fano resonance appears, and under the LCP and RCP illumination, an obvious chirality can be measured (Fig.3c).

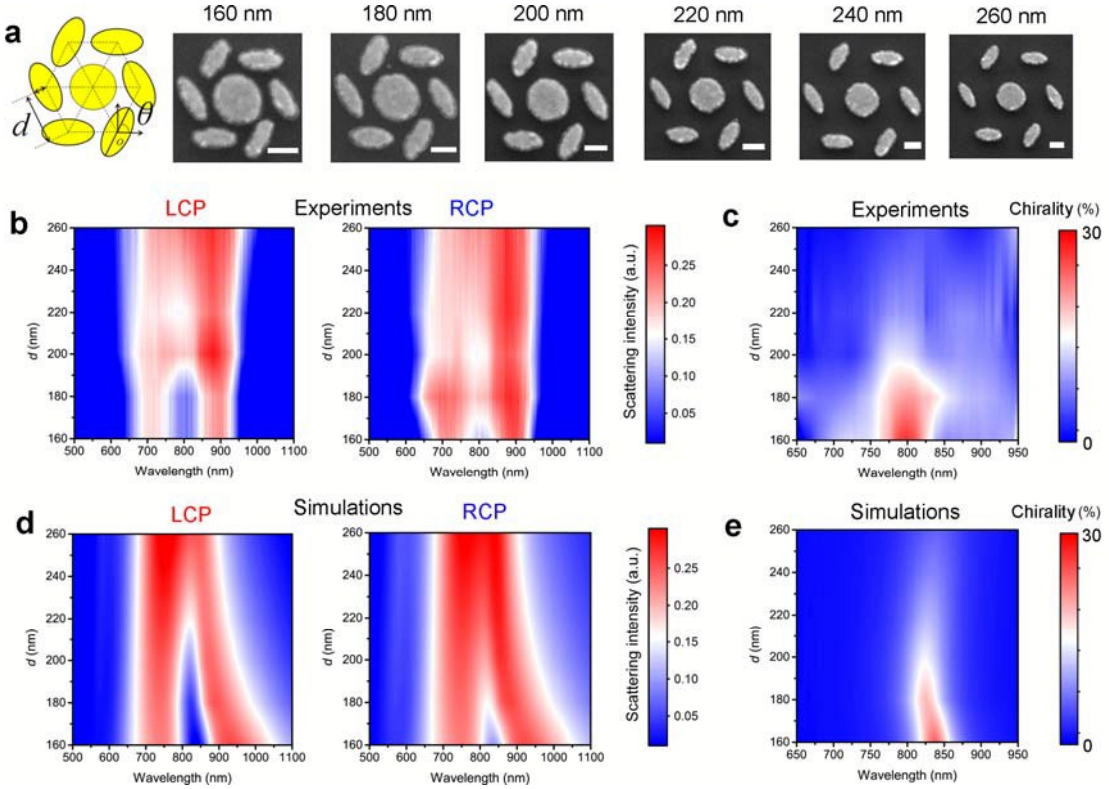

Figure 3. (a) Schematic of the chiral heptamer and SEM images for different inter-particle distance *d* that changed from 160 to 260 nm. (b-c) Experimental scattering intensity for each of the heptamer under LCP and RCP illumination, and corresponding chirality which reaches ~30% when *d*=160 nm. (d-e) Scattering cross section calculated using FEM simulations with different inter-particle distances for LCP and RCP excitation and the resulting chirality. The scale bar is 200

nm.

The chirality increased with the increasing of the Fano resonance strength, which is sensitive to the inter-particle distance *d*. With the distance *d* decreases to 160 nm, the maximum chirality ~30% is measured. The FEM simulations (Fig.3d and 3e) have a good agreement with the experiment observation, and indicating that with an even smaller inter-particle distance, our chirality based on the planar plasmonic nanostructure can reach its theoretical up limit. In order to explore the mechanism of this Fano enhanced chirality, we use the coupled dipole approximation (CDA) model and multipole mode expansion method to analyze this observed chirality.

Discussion

Dipole moment of surrounding ellipses. The CDA[4, 6, 38] model that we proposed provides a quantitative description of the dipole moments of the ellipses in the oligomer structure.(See Text S2 and S3 in the Supplementary Information) With this model, the magnitudes of the dipole moments along the major (or minor) axes of the six ellipses can be calculated and shown in Fig. 4a and 4b. We notice that for LCP excitation, the dipole moments along the minor axes are much smaller than along the major axis at the Fano resonance, while under RCP excitation, the dipole moments along the two axes become comparable. To further understand the dipole moment differences, we plot snapshots of the surface charge distributions (obtained by FEM) at the Fano resonance for LCP and RCP excitation in Figs. 4c and 4d.

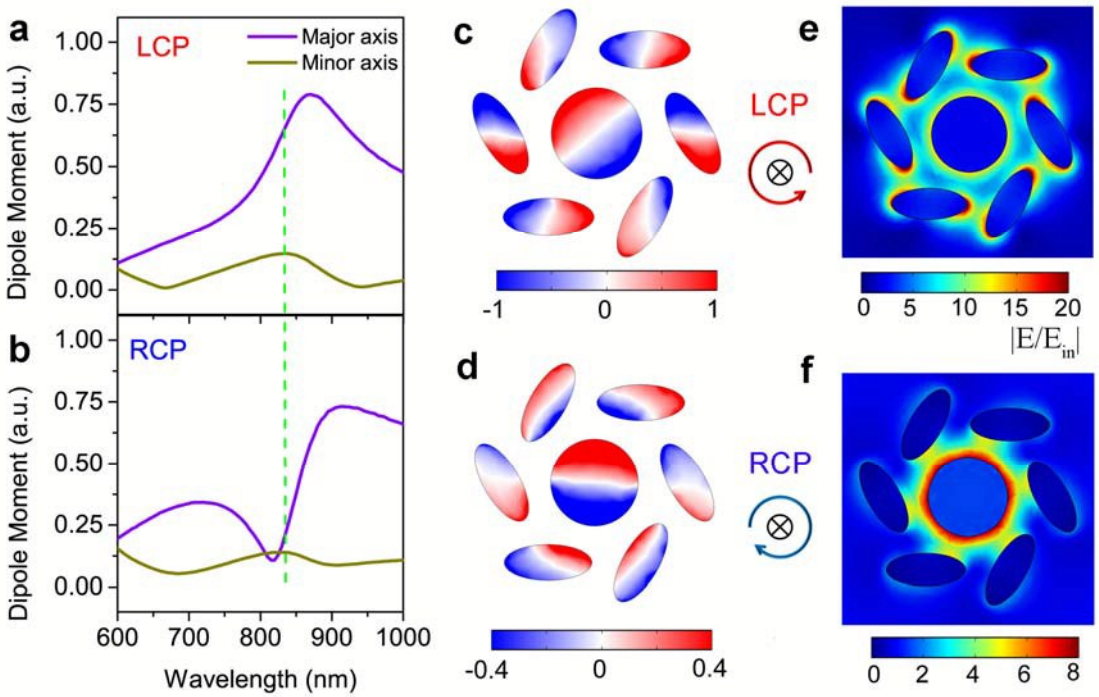

Figure 4. The dipole moments along the major and minor axis of the ellipse as a function of wavelength under (a) LCP and (b) RCP, respectively. The blue dashed lines show the wavelength position of the Fano resonance. FEM simulated surface charge (c,d) and electric field (e,f) distributions at the Fano resonance under LCP and RCP illuminations.

Plasmonic Fano interference is confirmed by the opposite alignment of the electric dipoles of the center disk and surrounding ellipses for both LCP and RCP. However, the nature of the polarization of the surrounding ellipses is different: for LCP, the polarization of the ellipses is predominantly along the major axis; while for RCP, the polarization is both along the major and minor axes. The calculated electric field distributions (Figs. 4e and 4f) give further explanations for this difference. For LCP, the strong coupling between adjacent ellipses leads to alignment of the dipoles along the major axis. For RCP, the strong couplings with the center disk induce a significant polarization also along the minor axes of the ellipses.

The origin of Fano induced optical chirality. To clarify which plasmonic modes are

responsible for the optical chirality, we use the multipole expansion method[39, 40] to analyze the plasmon modes. The total scattering power can be expanded as the sum of multipolar emitters:

$$I = \frac{\omega^4}{12\pi\varepsilon_0\varepsilon_r c^3}|\boldsymbol{p}|^2 + \frac{\omega^4}{12\pi\varepsilon_0\varepsilon_r c^5}|\boldsymbol{m}|^2 + \frac{\omega^6}{12\pi\varepsilon_0\varepsilon_r c^7}|\boldsymbol{T}|^2 - \frac{i\omega^5}{12\pi\varepsilon_0\varepsilon_r c^5}(\boldsymbol{p}^*\cdot\boldsymbol{T} - \boldsymbol{p}\cdot\boldsymbol{T}^*) + \frac{\omega^6}{160\pi\varepsilon_0\varepsilon_r c^5}\sum|Q_{\alpha\beta}|^2 + \frac{\omega^5}{160\pi\varepsilon_0\varepsilon_r c^7}\sum|M_{\alpha\beta}|^2 \quad (1)$$

where c is the speed of light, ω is the frequency and $\alpha, \beta = x, y, z$. The first two terms correspond to the bright electric and magnetic dipolar modes. The third term corresponds to scattering from a bright toroidal dipolar mode. The fourth term accounts for the interference between the electric and toroidal dipolar modes. The fifth and sixth terms are the contributions from dark electric and magnetic quadrupoles. The multipolar moments in Eq. (1) can be obtained from the calculated electric dipolar polarizations of each particle (See Text S4 in the Supplementary Information). The radiation powers from each term as a function of wavelength for LCP and RCP excitation are shown in Fig. 5. For both LCP and RCP incidence, the scattering powers from the magnetic dipole and the electric quadrupole are zero. The scattering powers from the electric dipole are similar for both polarizations in the entire range of wavelengths. The major differences between LCP and RCP are in the contributions from the dark magnetic quadrupole and the electrical toroidal dipole modes which peak at the Fano resonance for LCP. The electric-toroidal interference term is also different with a negligible contribution at the Fano resonance for RCP. From this decomposition, we can clearly see that the chirality in the scattering spectra arises from the excitation of magnetic quadrupolar and toroidal dipolar modes.

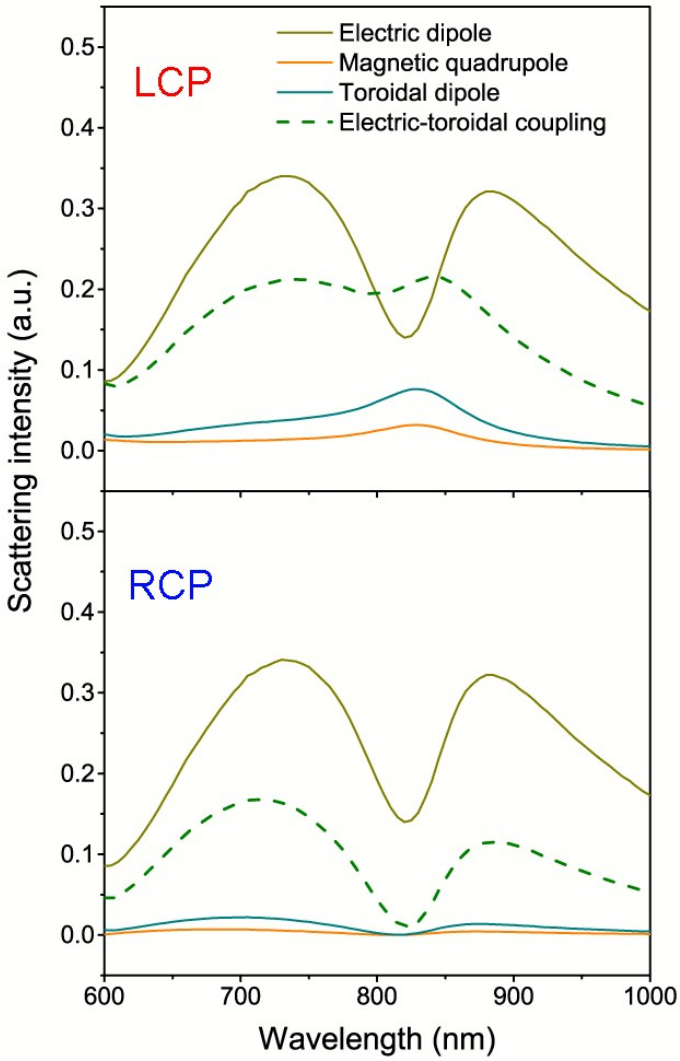

Figure 5. Multipolar contributions to the scattering for LCP and RCP incidence. The magnetic dipole and the electric quadrupole are not shown because they are zero. The electric dipole possesses the same scattering power in the entire range of wavelength, while the magnetic quadrupole, the toroidal dipole, and the electric-toroidal coupling show significant differences between LCP and RCP illumination.

In conclusion, we have demonstrated that plasmonic Fano resonances can be utilized to strongly enhance the chiral response of planar plasmonic oligomer nanostructure. The measured chiral response of the heptamer can reach the maximum

around 30% when the inter-disk distance is 160 nm and with the largest structure symmetry breaking. A near-field analysis reveals that the chirality enhancement is induced by the different excitation efficiency of dipole modes along the major and minor axis of the six satellite ellipses. Using a multipolar mode expansion, we further show that the origin of the enhanced chirality is a plasmonic Fano resonance caused by the excitation of magnetic quadrupolar and electric toroidal dipolar modes. Our designed Fano oligomer configuration and analysis method provide a convenient platform for the further optimization of Fano resonant oligomers for strong chiral optical response with potential applications in biosensing, metasurface, and other nanophotonics applications.

Methods

Sample preparation.

The planar nanostructures with different gaps and rotation angles were fabricated using electron-beam lithography (EBL) with a positive resist (PMMA) on a Si/SiO2 substrate. The Au structures were deposited by electron beam evaporation and followed by a standard lift-off procedure.

Numerical simulations.

The finite element solver (COMSOL) was used to simulate the scattering cross section of the fabricated nanostructures. The simulation domain includes the structure with perfect matched layers in all directions. The Au dielectric function was obtained from the experimental data of Johnson and Christy, [37] and the refractive index of SiO_2

is n=1.45. For the calculation, the electromagnetic fields of the Au nanostructures with the substrate were simulated.

Acknowledgements

This work was supported by National Science Foundation of China (Grant No. 11374023, 61422501 and 61521004), the National Basic Research Program of China (973 Program, Grant No. 2015CB932403), and Beijing Natural Science Foundation (Grant No. L140007). Foundation for the Author of National Excellent Doctoral Dissertation of PR China (Grant No.201420), National Program for Support of Top-notch Young Professionals.

References

1. Fan JA, *et al.* Self-assembled plasmonic nanoparticle clusters. *Science* **328**, 1135-1138 (2010).
2. Luk'yanchuk B, *et al.* The Fano resonance in plasmonic nanostructures and metamaterials. *Nat Mater* **9**, 707-715 (2010).
3. Lovera A, Gallinet B, Nordlander P, Martin OJ. Mechanisms of Fano resonances in coupled plasmonic systems. *Acs Nano* **7**, 4527-4536 (2013).
4. Auguié B, Barnes W. Collective Resonances in Gold Nanoparticle Arrays. *Phys Rev Lett* **101**, 143902 (2008).
5. Lévêque G, Martin OJF. Narrow-Band Multiresonant Plasmon Nanostructure for the Coherent Control of Light: An Optical Analog of the Xylophone. *Phys Rev Lett* **100**, 117402 (2008).
6. Lu X, *et al.* Circular dichroism from single plasmonic nanostructures with extrinsic chirality. *Nanoscale* **6**, 14244-14253 (2014).
7. Valev VK, Baumberg JJ, Sibilia C, Verbiest T. Chirality and chiroptical effects in plasmonic nanostructures: fundamentals, recent progress, and outlook. *Adv Mater* **25**, 2517-2534 (2013).

8. Shen X*, et al.* Three-dimensional plasmonic chiral tetramers assembled by DNA origami. *Nano Lett* **13**, 2128-2133 (2013).

9. Hentschel M, Schäferling M, Metzger B, Giessen H. Plasmonic diastereomers: adding up chiral centers. *Nano Lett* **13**, 600-606 (2013).

10. Yoo S, Park QH. Chiral Light-Matter Interaction in Optical Resonators. *Phys Rev Lett* **114**, 203003 (2015).

11. Tang Y, Cohen AE. Optical Chirality and Its Interaction with Matter. *Phys Rev Lett* **104**, 163901 (2010).

12. Gansel JK*, et al.* Gold helix photonic metamaterial as broadband circular polarizer. *Science* **325**, 1513-1515 (2009).

13. Cui Y, Kang L, Lan S, Rodrigues S, Cai W. Giant chiral optical response from a twisted-arc metamaterial. *Nano Lett* **14**, 1021-1025 (2014).

14. Hentschel M, Schäferling M, Weiss T, Liu N, Giessen H. Three-dimensional chiral plasmonic oligomers. *Nano Lett* **12**, 2542-2547 (2012).

15. Frank B*, et al.* Large-area 3D chiral plasmonic structures. *Acs Nano* **7**, 6321-6329 (2013).

16. Ma W*, et al.* Attomolar DNA detection with chiral nanorod assemblies. *Nat Commun* **4**, 2689 (2013).

17. Yan W*, et al.* Self-assembly of chiral nanoparticle pyramids with strong R/S optical activity. *J Am Chem Soc* **134**, 15114-15121 (2012).

18. Plum E, Fedotov VA, Schwanecke AS, Zheludev NI, Chen Y. Giant optical gyrotropy due to electromagnetic coupling. *Appl Phys Lett* **90**, 223113 (2007).

19. Kuwata-Gonokami M*, et al.* Giant Optical Activity in Quasi-Two-Dimensional Planar Nanostructures. *Phys Rev Lett* **95**, 227401 (2005).

20. Valev VK*, et al.* Plasmonic Ratchet Wheels: Switching Circular Dichroism by Arranging Chiral Nanostructures. *Nano Lett* **9**, 3945-3948 (2009).

21. Narushima T, Okamoto H. Circular dichroism nano-imaging of two-dimensional chiral metal nanostructures. *Phys Chem Chem Phys* **15**, 13805-13809 (2013).

22. Decker M, Klein MW, Wegener M, Linden S. Circular dichroism of planar chiral magnetic metamaterials. *Opt Lett* **32**, 856-858 (2007).

23. Fedotov V, Mladyonov P, Prosvirnin S, Rogacheva A, Chen Y, Zheludev N. Asymmetric Propagation of Electromagnetic Waves through a Planar Chiral Structure. *Phys Rev Lett* **97**, 167401 (2006).

24. Plum E, Liu XX, Fedotov V, Chen Y, Tsai D, Zheludev N. Metamaterials: Optical Activity without Chirality. *Phys Rev Lett* **102**, 113902 (2009).

25. Zhou Z-K*, et al.* Tuning gold nanorod-nanoparticle hybrids into plasmonic Fano resonance for dramatically enhanced light emission and transmission. *Nano Lett* **11**, 49-55 (2010).

26. Hentschel M, Saliba M, Vogelgesang R, Giessen H, Alivisatos AP, Liu N. Transition from isolated to collective modes in plasmonic oligomers. *Nano Lett* **10**, 2721-2726 (2010).

27. Zhao J, Zhang C, Braun PV, Giessen H. Large-area low-cost plasmonic nanostructures in the NIR for Fano resonant sensing. *Adv Mater* **24**, OP247-252 (2012).

28. Hao F, Sonnefraud Y, Dorpe PV, Maier SA, Halas NJ, Nordlander P. Symmetry breaking in plasmonic nanocavities: subradiant LSPR sensing and a tunable Fano resonance. *Nano Lett* **8**, 3983-3988 (2008).

29. Fan Z, Govorov AO. Chiral nanocrystals: plasmonic spectra and circular dichroism. *Nano Lett* **12**, 3283-3289 (2012).

30. Zhang Y, Zhen Y-R, Neumann O, Day JK, Nordlander P, Halas NJ. Coherent anti-Stokes Raman scattering with single-molecule sensitivity using a plasmonic Fano resonance. *Nat Commun* **5**, 4424 (2014).

31. Ye J*, et al.* Plasmonic nanoclusters: near field properties of the Fano resonance interrogated with SERS. *Nano Lett* **12**, 1660-1667 (2012).

32. Fan P, Yu Z, Fan S, Brongersma ML. Optical Fano resonance of an individual semiconductor nanostructure. *Nat Mater* **13**, 471-475 (2014).

33. Fang Z, Liu Z, Wang Y, Ajayan PM, Nordlander P, Halas NJ. Graphene-antenna sandwich photodetector. *Nano Lett* **12**, 3808-3813 (2012).

34. Kroner M*, et al.* The nonlinear Fano effect. *Nature* **451**, 311-314 (2008).

35. Zhang W, Govorov AO, Bryant GW. Semiconductor-metal nanoparticle molecules: Hybrid excitons and the nonlinear Fano effect. *Phys Rev Lett* **97**, 146804 (2006).

36. Fedotov VA, Schwanecke AS, Zheludev NI, Khardikov VV, Prosvirnin SL. Asymmetric transmission of light and enantiomerically sensitive plasmon resonance in planar chiral nanostructures. *Nano Lett* **7**, 1996-1999 (2007).

37. Johnson PB, Christy RW. Optical Constants of the Noble Metals. *Phys Rev B* **6**, 4370-4379 (1972).

38. Fang Z, Cai J, Yan Z, Nordlander P, Halas NJ, Zhu X. Removing a wedge from a metallic nanodisk reveals a fano resonance. *Nano Lett* **11**, 4475-4479 (2011).

39. Kaelberer T, Fedotov VA, Papasimakis N, Tsai DP, Zheludev NI. Toroidal Dipolar Response in a Metamaterial. *Science* **330**, 1510-1512 (2010).

40. Radescu E, Vaman G. Exact calculation of the angular momentum loss, recoil force, and radiation intensity for an arbitrary source in terms of electric, magnetic, and toroid multipoles. *Phys Rev E* **65**, 046609 (2002).